arXiv:1408.4740v3 [cond-mat.mes-hall] 30 Oct 2015

Capacitively coupled singlet-triplet qubits in the double charge resonant regime

V. Srinivasa[1, 2, 3, *] and J. M. Taylor[1, 2, 4]

[1] *Joint Quantum Institute, University of Maryland, College Park, Maryland 20742, USA*
[2] *National Institute of Standards and Technology, Gaithersburg, Maryland 20899, USA*
[3] *Laboratory for Physical Sciences, College Park, Maryland 20740, USA*
[4] *Joint Center for Quantum Information and Computer Science, University of Maryland, College Park, Maryland 20742, USA*

We investigate a method for entangling two singlet-triplet qubits in adjacent double quantum dots via capacitive interactions. In contrast to prior work, here we focus on a regime with strong interactions between the qubits. The interplay of the interaction energy and simultaneous large detunings for both double dots gives rise to the "double charge resonant" regime, in which the unpolarized (1111) and fully polarized (0202) four-electron states in the absence of interqubit tunneling are near degeneracy, while being energetically well-separated from the partially polarized (0211 and 1102) states. A rapid controlled-phase gate may be realized by combining time evolution in this regime in the presence of intraqubit tunneling and the interqubit Coulomb interaction with refocusing π pulses that swap the singly occupied singlet and triplet states of the two qubits via, e.g., magnetic gradients. We calculate the fidelity of this entangling gate, incorporating models for two types of noise – charge fluctuations in the single-qubit detunings and charge relaxation within the low-energy subspace via electron-phonon interaction – and identify parameter regimes that optimize the fidelity. The rates of phonon-induced decay for pairs of GaAs or Si double quantum dots vary with the sizes of the dipolar and quadrupolar contributions and are several orders of magnitude smaller for Si, leading to high theoretical gate fidelities for coupled singlet-triplet qubits in Si dots. We also consider the dependence of the capacitive coupling on the relative orientation of the double dots and find that a linear geometry provides the fastest potential gate.

I. INTRODUCTION

Electrons spins confined within semiconductor quantum dots form the basis of a highly controllable and potentially scalable approach to solid-state quantum information processing.[1–5] The encoding of spin quantum bits (qubits) in two-electron singlet and triplet states of a double quantum dot[2,6–8] enables rapid, universal manipulation via tuning of the singlet-triplet (exchange) splitting through electrical control over the double-dot potential[9] combined with static magnetic field gradients,[10,11] without requiring time-dependent magnetic fields and while simultaneously providing protection against errors induced by hyperfine interaction.[8,9,12–18] Coherent control of singlet-triplet qubits has been experimentally demonstrated in the context of both single-qubit manipulation[9,11,17,19–21] and two-qubit entanglement.[22,23]

For a pair of singlet-triplet qubits coupled via tunneling, the effective exchange interaction can be used to carry out two-qubit gates;[7,24–28] however, this approach typically requires an accompanying mechanism for suppressing errors due to leakage out of the qubit subspace during gate operation. Alternatively, two singlet-triplet qubits in adjacent double dots may be entangled via capacitive coupling.[2,22,23,29–36] In this case, interqubit tunneling is absent and the entanglement instead originates from the Coulomb interaction of the multipole moments associated with the different charge distributions of the singlet and triplet states.[15] The spin-dependent charge dipole moments of spatially separated singlet-triplet qubits can also be coupled to microwaves, enabling long-range, high-frequency gating.[37,38] Nevertheless, realizing robust entangling gates in the presence of the charge-based decoherence mechanisms typically existing in the solid state, including both dephasing[8,15,39–42] and relaxation via, e.g., coupling to phonons,[8,12,43–48] remains challenging.

Here, we consider a pair of capacitively coupled singlet-triplet qubits in the absence of interqubit tunneling. In contrast to the repulsive interqubit dipole-dipole interaction originally considered in Ref. 2, we focus specifically on the case of an attractive dipole-dipole interaction, implemented by adjusting via external gate voltages the energy detunings between the singly and doubly occupied two-electron charge configurations such that they are large for both double dots. The interplay of these large detunings and the Coulomb interaction energy gives rise to the "double charge resonant" regime, as we describe below.

Combining time evolution in this regime with single-qubit π pulses that swap the singly occupied singlet and triplet states of both qubits using, e.g., static magnetic gradients[23] leads to a controlled π-phase (or controlled-Z) entangling gate. As a consequence of the attractive dipole-dipole interaction, increasing the speed of this gate simultaneously decreases the gate error due to charge noise. We calculate the gate fidelity in the presence of charge fluctuations in the double-dot detunings and identify gate voltages and coupling strengths at which the fidelity is optimized. We then investigate charge relaxation due to electron-phonon coupling for both GaAs and Si double quantum dots in linear and purely quadrupolar dot configurations and determine the effects of both

this relaxation and fast charge noise on the gate fidelity. Finally, we consider the geometry dependence of the interqubit capacitive coupling and identify the linear geometry as a configuration that maximizes the gate speed.

II. MODEL AND DOUBLE CHARGE RESONANT REGIME

We consider two singlet-triplet qubits, realized within a pair of adjacent two-electron double quantum dots [Fig. 1(a)] with only the lowest orbital level of each dot taken into account. Each two-electron double dot encodes one qubit. As in Ref. 2, we initially assume a linear geometry in which the tunnel barriers are adjusted via gates such that tunneling occurs only between the dots within each qubit, while adjacent dots belonging to different qubits are coupled purely capacitively. We can write a Hubbard Hamiltonian for the system[49] as $H_{\rm hub} = H_a + H_b + H_{\rm int}$, where

$$H_\alpha = H_{\alpha n} + H_{\alpha t}, \tag{1}$$

$$H_{\alpha n} = \sum_{i=1,2}\left[\epsilon_{\alpha i} n_{\alpha i} + \frac{U_\alpha}{2} n_{\alpha i}(n_{\alpha i}-1)\right] + V_\alpha n_{\alpha 1} n_{\alpha 2}, \tag{2}$$

$$H_{\alpha t} = \sum_{i\neq j}\sum_{\sigma} t_\alpha c^\dagger_{\alpha i\sigma} c_{\alpha j\sigma}, \tag{3}$$

is the Hamiltonian for double dot $\alpha = a, b$, and $H_{\rm int}$ is the capacitive interaction between the double dots. For simplicity, we initially include only the dominant interaction term for the linear geometry we consider,

$$H_{\rm int} = U_{ab} n_{a2} n_{b1}. \tag{4}$$

Equations (2) and (4) are expressed in terms of the electron number operators $n_{\alpha i} = \sum_\sigma n_{\alpha i\sigma} = \sum_\sigma c^\dagger_{\alpha i\sigma} c_{\alpha i\sigma}$, where $c^\dagger_{\alpha i\sigma}$ creates an electron in dot i of qubit α with spin $\sigma = \uparrow, \downarrow$ and orbital energy $\epsilon_{\alpha i}$. These terms determine the energy of each four-electron charge configuration $|n_{a1}\ n_{a2}\ n_{b1}\ n_{b2}\rangle$ in the absence of interdot tunneling. The quantities U_α and V_α are the Coulomb repulsion energies for two electrons in the same dot and in different dots within qubit α, respectively. $H_{\alpha t}$ couples the double-dot charge configurations $(n_{\alpha 1}, n_{\alpha 2})$ via tunneling, and t_α denotes the tunneling amplitude for double dot α. As discussed in Refs. 2 and 8, each double dot can be described in the two-electron regime as an effective three-level system with a state space spanned by

$$|T_{11}\rangle \equiv |(1,1)\, T_0\rangle = \frac{1}{\sqrt{2}}\left(c^\dagger_{1\uparrow}c^\dagger_{2\downarrow} + c^\dagger_{1\downarrow}c^\dagger_{2\uparrow}\right)|0\rangle, \tag{5}$$

$$|S_{11}\rangle \equiv |(1,1)\, S\rangle = \frac{1}{\sqrt{2}}\left(c^\dagger_{1\uparrow}c^\dagger_{2\downarrow} - c^\dagger_{1\downarrow}c^\dagger_{2\uparrow}\right)|0\rangle, \tag{6}$$

$$|S_{02}\rangle \equiv |(0,2)\, S\rangle = c^\dagger_{2\uparrow}c^\dagger_{2\downarrow}|0\rangle, \tag{7}$$

where the qubit index α has been suppressed for clarity.

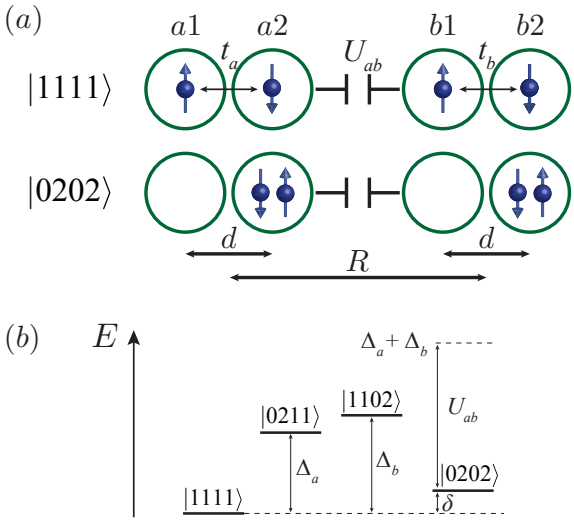

Figure 1. (a) Schematic diagram of capacitively coupled double quantum dots in the charge states $|1111\rangle$ and $|0202\rangle$. The interdot spacing within each double dot is d, and the separation between the centers of the double dots is R. (b) Energy level diagram for the main four-electron charge configurations considered in the present work, illustrating the double charge resonant regime.

In our analysis of the capacitively coupled double-dot pair system, we focus on the four-electron charge subspaces $|1111\rangle$, $|0202\rangle$, $|1102\rangle$, and $|0211\rangle$. Noting that $H_{\rm hub}$ conserves both the total spin and the total z component of spin and that $H_{\alpha t}$ couples only the two-electron singlet states $|S_{11}\rangle$ and $|S_{02}\rangle$ within double dot α, we may consider the subspace spanned by product states of the form $|S_a, S_b\rangle \equiv |S_a\rangle \otimes |S_b\rangle$, where $|S_\alpha\rangle \in \{|S_{11}\rangle, |S_{02}\rangle\}$ for $\alpha = a, b$. In the basis $\{|S_{11}, S_{11}\rangle, |S_{02}, S_{02}\rangle, |S_{11}, S_{02}\rangle, |S_{02}, S_{11}\rangle\}$, the Hamiltonian has the representation

$$H_{\rm hub} = \begin{pmatrix} 0 & 0 & \sqrt{2}t_b & \sqrt{2}t_a \\ 0 & \delta & \sqrt{2}t_a & \sqrt{2}t_b \\ \sqrt{2}t_b & \sqrt{2}t_a & \Delta_b & 0 \\ \sqrt{2}t_a & \sqrt{2}t_b & 0 & \Delta_a \end{pmatrix}, \tag{8}$$

where $\Delta_a \equiv -\epsilon_a + U_a - V_a + U_{ab}$ and $\Delta_b \equiv -\epsilon_b + U_b - V_b - U_{ab}$ are the effective energy detunings between $|S_{11}\rangle$ and $|S_{02}\rangle$ for double dots a and b, respectively (accounting for coupling to the other double dot), $\epsilon_\alpha \equiv \epsilon_{\alpha 1} - \epsilon_{\alpha 2}$, and $\delta \equiv \Delta_a + \Delta_b - U_{ab}$ is the energy difference between $|S_{11}, S_{11}\rangle$ and $|S_{02}, S_{02}\rangle$. The detunings Δ_α are controlled via tuning of the on-site energies via gate voltages, which set ϵ_a and ϵ_b.

The controlled-phase gate for two singlet-triplet qubits discussed in Sec. III involves tunneling from $|S_{11}\rangle$ to $|S_{02}\rangle$ for $\alpha = a, b$, which simultaneously induces dipole moments in both double dots. Given that the interqubit Coulomb interaction strength $U_{ab} > 0$, the regime of interest for the operation of this gate is that in which

$\Delta_\alpha \gg \delta > 0$ for $\alpha = a, b$, so that $|S_{11}, S_{11}\rangle$ is lower in energy than $|S_{02}, S_{02}\rangle$, while $|S_{11}, S_{11}\rangle$ and $|S_{02}, S_{02}\rangle$ are energetically well-separated from $|S_{11}, S_{02}\rangle$ and $|S_{02}, S_{11}\rangle$ [Fig. 1(b)]. We refer to this regime as the "double charge resonant regime," as the attractive interaction between the dipole moments of the two double dots in the state $|S_{02}, S_{02}\rangle$ effectively brings it into near-resonance with $|S_{11}, S_{11}\rangle$. Note that this regime is not accessible in the scenario originally studied in Ref. 2, where the state $|S_{02}, S_{20}\rangle$ is considered instead of $|S_{02}, S_{02}\rangle$ and the interqubit Coulomb interaction between the dipole moments is repulsive.

We show in Sec. III that, in contrast to the nonresonant regime of Ref. 2, the double charge resonant regime enables a controlled-phase gate to be generated by dynamics within an effective low-energy subspace derived from $|S_{11}, S_{11}\rangle$ and $|S_{02}, S_{02}\rangle$. In order to compare two-qubit phase gates in the nonresonant and double charge resonant regimes, we now estimate the scaling of the phase gate errors in the presence of detuning noise. Using Eq. (8), we calculate the fourth-order energy shift for the state $|S_{11}, S_{11}\rangle$ due to the interqubit capacitive coupling (i.e., the additional energy shift for $U_{ab} \neq 0$), which gives the rate of the phase gate. For the nonresonant regime, the Hamiltonian has the same form as Eq. (8) with the replacements $|S_{02}, S_{02}\rangle \to |S_{02}, S_{20}\rangle$, $|S_{11}, S_{02}\rangle \to |S_{11}, S_{20}\rangle$, and $\delta = \Delta_a + \Delta_b + U_{ab}$ (here, $\Delta_b \equiv \epsilon_b + U_b - V_b + U_{ab}$). Assuming $\Delta_a = \Delta_b \equiv \Delta$ and $t_a = t_b \equiv t$ for simplicity, we find a phase gate rate $\varepsilon_{1111} = 8t^4 (\delta - 2\Delta)/\Delta^3\delta$.

Setting $\Delta' = \Delta + \xi$, where ξ represents classical, static, Gaussian-distributed noise in the single-qubit detunings due to gate voltage fluctuations,[42] we can write the nontrivial phase factor acquired by the state derived from $|S_{11}, S_{11}\rangle$ for $U_{ab} \neq 0$ as $e^{i\phi'}$, with $\phi' = \phi_0 + \phi_\xi$. Here, $\phi_0 \equiv \varepsilon_{1111}\tau_{\text{gate}}$ is the phase acquired during the gate time τ_{gate} in the absence of noise and $\phi_\xi \approx (4t^2/\Delta^2)\,\xi\tau_{\text{gate}}$ represents the phase fluctuations, approximated using the second-order energy shift. Averaging over the noise gives $\left\langle e^{i\phi'}\right\rangle = e^{-\Gamma_\xi^2\tau^2} e^{i\phi_0} \approx \left(1 - \Gamma_\xi^2\tau^2\right) e^{i\phi_0}$ with $\Gamma_\xi \sim t^2/\Delta^2 T_{2,\xi}^*$ ($T_{2,\xi}^*$ denotes the dephasing time associated with the charge fluctuations ξ), so that the phase gate error can be approximated as $\text{err} \approx \Gamma_\xi^2\tau_{\text{gate}}^2 \sim \delta^2\Delta^2/t^4\,(\delta - 2\Delta)^2\, T_{2,\xi}^{*2}$. For the nonresonant regime, $\delta = 2\Delta + U_{ab}$ and $\text{err} \sim (\Delta^2/t^2)\,(1 + 2\Delta/U_{ab})^2 / \left(tT_{2,\xi}^*\right)^2$, while for the double charge resonant regime, $\delta = 2\Delta - U_{ab}$ and $\text{err} \sim \delta^2/t^2 \left(tT_{2,\xi}^*\right)^2$. Thus, the phase gate error due to gate voltage fluctuations has the scaling $\sim \Delta^2/t^2$ for the nonresonant regime, which is unfavorable for suppressing errors arising from dipole transitions to $|S_{11}, S_{20}\rangle$ and $|S_{02}, S_{11}\rangle$ by keeping Δ/t large. On the other hand, the error scales as $\sim \delta^2/t^2$ in the double charge resonant regime, so that faster gates (corresponding to stronger coupling U_{ab} and therefore smaller δ for fixed Δ) are also associated with smaller error.

We now proceed with a more detailed analysis of the double charge resonant regime and consider the low-energy effective Hamiltonian in the subspace $\{|S_{11}, S_{11}\rangle, |S_{02}, S_{02}\rangle\}$. Applying a Schrieffer-Wolff transformation of the form $\tilde{H} = e^{\lambda A} H_{\text{hub}} e^{-\lambda A}$ with $\lambda \propto t_\alpha$ (assuming $t_a \sim t_b$) to the Hamiltonian in Eq. (8), we choose A such that the coupling to the higher-energy states $|S_{11}, S_{02}\rangle$ and $|S_{02}, S_{11}\rangle$ is eliminated up to $\mathcal{O}(\lambda^2)$. Expressions for the basis states resulting from this transformation are given in Appendix A.

Defining $\sigma_z = \left|\widetilde{S_{11}, S_{11}}\right\rangle\left\langle\widetilde{S_{11}, S_{11}}\right| - \left|\widetilde{S_{02}, S_{02}}\right\rangle\left\langle\widetilde{S_{02}, S_{02}}\right|$, the effective Hamiltonian within the transformed subspace is

$$H_{\text{eff}} = -\left(J_a + J_b - \frac{j_d}{2}\right)\mathbf{1} - \frac{j_d}{2}\sigma_z - j_x\sigma_x, \tag{9}$$

where, in terms of the charge admixture parameters $\eta_\alpha \equiv t_\alpha/\Delta_\alpha$, δ, and the difference of the detunings $\Delta_d \equiv \Delta_a - \Delta_b$,

$$J_a \equiv \eta_a^2\,(U_{ab} + \delta + \Delta_d), \tag{10}$$

$$J_b \equiv \eta_b^2\,(U_{ab} + \delta - \Delta_d), \tag{11}$$

$$j_d \equiv \delta - 2\left(J_a \frac{\delta + \Delta_d}{U_{ab} - \delta - \Delta_d} + J_b \frac{\delta - \Delta_d}{U_{ab} - \delta + \Delta_d}\right), \tag{12}$$

$$j_x \equiv 2\eta_a\eta_b U_{ab}\left[1 + \delta\left(\frac{1}{U_{ab} - \delta - \Delta_d} + \frac{1}{U_{ab} - \delta + \Delta_d}\right)\right]. \tag{13}$$

Diagonalization of Eq. (9) yields the eigenstates $|g\rangle = \cos\theta\left|\widetilde{S_{11}, S_{11}}\right\rangle - \sin\theta\left|\widetilde{S_{02}, S_{02}}\right\rangle$ and $|e\rangle = \sin\theta\left|\widetilde{S_{11}, S_{11}}\right\rangle + \cos\theta\left|\widetilde{S_{02}, S_{02}}\right\rangle$, where

$$\tan\theta = \frac{j_d - \Omega}{2j_x} \tag{14}$$

and $\Omega \equiv E_e - E_g = \sqrt{j_d^2 + 4j_x^2}$ is the energy gap between $|g\rangle$ and $|e\rangle$. The spectrum of H_{eff} is shown in Fig. 2 as a function of δ for $U_{ab} = 200\ \mu\text{eV}$, $\Delta_d = 0$, and $\eta_a = \eta_b \equiv \eta_0 = 0.1$. An avoided crossing occurs at $\delta = 0$, i.e., when $|S_{11}, S_{11}\rangle$ and $|S_{02}, S_{02}\rangle$ are resonant. For $\delta \gg 0$, $|g\rangle \approx \left|\widetilde{S_{11}, S_{11}}\right\rangle$ and $|e\rangle \approx \left|\widetilde{S_{02}, S_{02}}\right\rangle$.

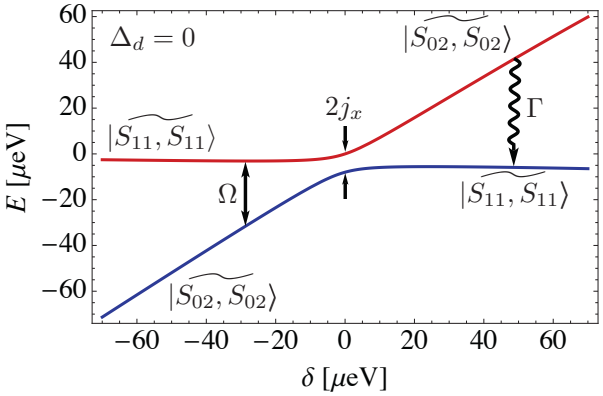

Figure 2. Spectrum of $H_{\rm eff}$ [Eq. (9)] as a function of δ for $U_{ab} = 200$ μeV, $\Delta_d = 0$, and $\eta_a = \eta_b \equiv \eta_0 = 0.1$.

III. CONTROLLED-PHASE GATE

The time evolution generated by the Hamiltonian $H_{\rm eff}$ [Eq. (9)] within the two-singlet subspace spanned by $\left\{\left|\widetilde{S_{11}, S_{11}}\right\rangle, \left|\widetilde{S_{02}, S_{02}}\right\rangle\right\}$ leads to a controlled-phase gate between the two singlet-triplet qubits that is based on capacitive coupling in the double charge resonant regime. In order to obtain this two-qubit entangling gate, we now incorporate the triplet states of the double dots [Eq. (5)] into the analysis. Since the full sequence for the controlled-phase gate also involves single-qubit rotations around two orthogonal axes, we consider the Hamiltonian $H_{\rm hub} + H_{aZ} + H_{bZ}$, where

$$H_{\alpha Z} = \frac{g\mu_B}{2} \sum_{i=1,2} \sum_{\sigma,\sigma'} c^\dagger_{\alpha i\sigma} \left(\mathbf{B}_{\alpha i} \cdot \boldsymbol{\sigma}_\alpha\right) c_{\alpha i\sigma'} \tag{15}$$

represents Zeeman coupling to magnetic fields $\mathbf{B}_{\alpha i}$ for double dot α (here, g is the effective electron g factor and μ_B denotes the Bohr magneton). Combining this Zeeman coupling with the spin-independent Hubbard term H_α [Eqs. (1)-(3)] that leads to the exchange J_α enables universal one-qubit control of singlet-triplet qubits.[2,7–9,11,17,19–21] In the basis $\{|T_{11}\rangle, |S_{11}\rangle, |S_{02}\rangle\}$ [Eqs. (5)-(7)], $H'_\alpha \equiv H_\alpha + H_{\alpha Z}$ takes the form[2,8]

$$H'_\alpha = \begin{pmatrix} 0 & \omega_{\alpha Z} & 0 \\ \omega_{\alpha Z} & 0 & \sqrt{2}t_\alpha \\ 0 & \sqrt{2}t_\alpha & \Delta_\alpha \end{pmatrix}, \tag{16}$$

where we have defined the energy associated with a static magnetic field gradient of magnitude $dB_\alpha \equiv (B_{\alpha 1} - B_{\alpha 2})/2$ along the single-spin quantization axis as $\omega_{\alpha Z} \equiv g\mu_B dB_\alpha$.

We initially consider the double charge resonant regime ($\Delta_\alpha \gg \delta$) in the limit $\omega_{\alpha Z} \to 0$ and keep only the term H_α in the Hamiltonian for double dot α. Elimination of the doubly occupied singlet state $|S_{02}\rangle$ gives the effective Hamiltonian $H_{\alpha J} \equiv -J_\alpha \left|\tilde{S}_{11}\right\rangle \left\langle\tilde{S}_{11}\right| = J_\alpha (Z_\alpha - \mathbf{1})/2$, where $Z \equiv |T_{11}\rangle\langle T_{11}| - \left|\tilde{S}_{11}\right\rangle \left\langle\tilde{S}_{11}\right|$, which generates a rotation around the z axis of the Bloch sphere for the singlet-triplet qubit.[2,8,9] Combining $H_{\alpha J}$ for $\alpha = a, b$ and $H_{\rm eff}$ [Eq. (9)] yields, in the two-qubit basis $\left\{|T_{11}, T_{11}\rangle, \left|\tilde{S}_{11}, T_{11}\right\rangle, \left|T_{11}, \tilde{S}_{11}\right\rangle, \left|\widetilde{S_{11}, S_{11}}\right\rangle, \left|\widetilde{S_{02}, S_{02}}\right\rangle\right\}$,

$$H_J = \left(\begin{array}{ccc|cc} 0 & & & & \\ & -J_a & & & \\ & & -J_b & & \\ \hline & & & -J_a - J_b & -j_x \\ & & & -j_x & -J_a - J_b + j_d \end{array}\right). \tag{17}$$

The dynamics generated by H_J are described by the operator

$$\hat{U}_J(\tau) \equiv e^{-iH_J\tau} = \left(\begin{array}{ccc|c} 1 & & & \\ & e^{iJ_a\tau} & & \\ & & e^{iJ_b\tau} & \\ \hline & & & e^{-iH_{\rm eff}\tau} \end{array}\right), \tag{18}$$

where

$$e^{-iH_{\rm eff}\tau} = e^{i(J_a + J_b - j_d/2)\tau} \left[\cos\left(\frac{\Omega\tau}{2}\right)\mathbf{1} + i\sin\left(\frac{\Omega\tau}{2}\right)\left(\frac{j_d}{\Omega}\sigma_z + \frac{2j_x}{\Omega}\sigma_x\right)\right]. \tag{19}$$

The gate $\hat{U}_J$ thus describes an oscillation between $\left|\widetilde{S_{11}, S_{11}}\right\rangle$ and $\left|\widetilde{S_{02}, S_{02}}\right\rangle$ with frequency Ω, together with z-axis rotations of the individual qubits. This evolution occurs in the double charge resonant regime illustrated in Figs. 1 and 2.

To obtain a controlled-phase gate using $\hat{U}_J$ that incorporates robustness to single-qubit exchange errors, we construct a gate sequence that includes spin-echo (refocusing) pulses.[50] For a singlet-triplet qubit, phase errors accumulated due to exchange fluctuations can be canceled via a π rotation about the x axis of the Bloch sphere,[2,51] and simultaneous π pulses can be applied to both qubits.[23] Since single-qubit x-axis rotations are generated by the terms H_{aZ} and H_{bZ} [see Eqs. (15) and (16)], the refocusing pulses are applied in the regime $\omega_{\alpha Z} \gg J_\alpha$ for $\alpha = a, b$. This regime can be reached by adjusting the double-dot detunings such that the $|0211\rangle$ and $|1102\rangle$ states are energetically closer than $|0202\rangle$ to the $|1111\rangle$ state, with $\Delta_\alpha \lesssim \left|\tilde{\delta}\right| - t_\alpha$ for $\alpha = a, b$ (here, we use a new symbol $\tilde{\delta}$ in order to indicate that the range of values of $\Delta_a + \Delta_b - U_{ab}$ is different from that of δ in the double charge resonant regime). The effective Hamiltonian is $H_Z \equiv \omega_Z (X_a + X_b) + \tilde{\delta} \left|\widetilde{S_{02}, S_{02}}\right\rangle \left\langle\widetilde{S_{02}, S_{02}}\right|$, where $X \equiv |T_{11}\rangle \left\langle\tilde{S}_{11}\right| + \left|\tilde{S}_{11}\right\rangle \langle T_{11}|$ and we choose $dB_a = dB_b$ for simplicity. The associated evolution is $e^{-iH_Z\tau}$, which for $\tau = \pi/2\omega_Z$ is equal to $R_\pi \equiv -X_a X_b + e^{-i\pi\tilde{\delta}/2\omega_Z} \left|\widetilde{S_{02}, S_{02}}\right\rangle \left\langle\widetilde{S_{02}, S_{02}}\right|$. We note that applying R_π results in the accumulation of a relative phase between the $|0202\rangle$ and $|1111\rangle$ charge subspaces.

The full sequence for the controlled-phase gate in terms of the exchange gate in the double charge resonant regime, $\hat{U}_J$, and the refocusing pulse gate, R_π, is given by

$$P_S e^{-i\phi} e^{-iH_{aJ}\tau_a} e^{-iH_{bJ}\tau_b} R_\pi \hat{U}_J(\tau_n) R_\pi \hat{U}_J(\tau_n) P_S = \begin{pmatrix} 1 & & & \\ & 1 & & \\ & & 1 & \\ & & & e^{2i\phi} \end{pmatrix}. \quad (20)$$

Here, $\tau_n = 2\pi n/\Omega$ and $\phi = (1 - j_d/\Omega)\, n\pi$, where n is an integer, $\tau_\alpha = \phi/J_\alpha$, and P_S is the projector onto the four-dimensional $|1111\rangle$ subspace spanned by $\left\{|T_{11}, T_{11}\rangle, \left|\tilde{S}_{11}, T_{11}\right\rangle, \left|T_{11}, \tilde{S}_{11}\right\rangle, \left|\widetilde{S_{11}, S_{11}}\right\rangle\right\}$. In the next section, we consider the controlled π-phase gate, which corresponds to $\phi = \pi/2$.

IV. CHARGE NOISE AND GATE FIDELITY

In practice, the performance of the controlled-phase gate in Eq. (20) is affected by charge noise.[8,15,40,42,52,53] We now investigate the effects of classical, Gaussian-distributed noise in δ and Δ_d due to gate voltage fluctuations and set $\delta' = \delta + \xi_s$, $\Delta_d' = \Delta_d + \xi_d$, where ξ_s and ξ_d are assumed to be uncorrelated and have the distributions $\rho_\beta(\xi_\beta) = e^{-\xi_\beta^2/2\sigma_\beta^2}/\sqrt{2\pi}\sigma_\beta$ with charge noise standard deviations σ_β for $\beta = s, d$. In what follows, we assume that R_π and the single-qubit rotations in Eq. (20) are ideal in order to focus on effects due to errors in $\hat{U}_J$, which is the gate derived from the capacitive interaction of the double dots in the double charge resonant regime. Errors due to residual magnetic gradient terms are discussed briefly at the end of this section.

We therefore consider the simpler gate sequence

$$U_\phi \equiv \hat{U}_J(\tau_n) R_\pi \hat{U}_J(\tau_n) = \begin{pmatrix} & & e^{i\phi} & \\ & 1 & & \\ 1 & & & \\ & & & e^{i\zeta} \\ e^{i\phi} & & & \end{pmatrix}, \quad (21)$$

where $\zeta = \left\{2(J_a + J_b - j_d)\, n/\Omega + 1 - \tilde{\delta}/2\omega_Z\right\}\pi$ and we have neglected a trivial global phase factor. Equation (21) represents the ideal gate sequence. We determine the gate sequence U_ϕ' in the presence of charge noise by expanding the terms in the Hamiltonian H_J [Eq. (17)], which are defined in Eqs. (10)-(13), up to second order in the fluctuations ξ_β. For $h = J_a, J_b, j_d, j_x$,

$$h' \equiv h(\delta', \Delta_d') \approx h(\delta, \Delta_d) + \left.\frac{\partial h}{\partial \delta'}\right|_0 \xi_s + \left.\frac{\partial h}{\partial \Delta_d'}\right|_0 \xi_d + \frac{1}{2}\left.\frac{\partial^2 h}{\partial \delta'^2}\right|_0 \xi_s^2 + \frac{1}{2}\left.\frac{\partial^2 h}{\partial \Delta_d'^2}\right|_0 \xi_d^2 + \left.\frac{\partial^2 h}{\partial \delta' \partial \Delta_d'}\right|_0 \xi_s \xi_d,$$

where we use the notation $|_0 \equiv |_{\delta'=\delta, \Delta_d'=\Delta_d}$. Substitution of these expressions into Eq. (18) then yields U_ϕ'.

For an initial state $|\psi_{in}\rangle$, we define the minimum fidelity as

$$F_{\min} = \left\langle \mathrm{Tr}\left[\hat{\rho}_{\mathrm{out}}^{(0)} \hat{\rho}_{\mathrm{out}}\right]\right\rangle_{\xi_s, \xi_d} = \int_{-\infty}^{\infty}\int_{-\infty}^{\infty} \mathrm{Tr}\left[\hat{\rho}_{\mathrm{out}}^{(0)} \hat{\rho}_{\mathrm{out}}\right] \times \rho_s(\xi_s)\, \rho_d(\xi_d)\, d\xi_s d\xi_d, \quad (22)$$

where $\hat{\rho}_{\mathrm{out}}^{(0)} \equiv U_\phi |\psi_{\mathrm{in}}\rangle \langle\psi_{\mathrm{in}}| U_\phi^\dagger$ is the final state after evolution under the ideal gate sequence and $\hat{\rho}_{\mathrm{out}} \equiv U_\phi' |\psi_{\mathrm{in}}\rangle \langle\psi_{\mathrm{in}}| U_\phi'^\dagger$ is the final state after the corresponding evolution in the presence of charge noise. We choose $|\psi_{\mathrm{in}}\rangle = \frac{1}{2}\left(|T_{11}, T_{11}\rangle + \left|\tilde{S}_{11}, T_{11}\right\rangle + \left|T_{11}, \tilde{S}_{11}\right\rangle + \left|\widetilde{S_{11}, S_{11}}\right\rangle\right)$ in order to maximize the error (see Appendix B) and assume that this state can be prepared without errors. $F_{\min}$ is then independent of ζ, as there is initially zero probability that the system is in the state $\left|\widetilde{S_{02}, S_{02}}\right\rangle$ [see Eq. (21)]. We find

$$\mathrm{Tr}\left[\hat{\rho}_{\mathrm{out}}^{(0)} \hat{\rho}_{\mathrm{out}}\right] = \cos^2\left[\frac{n\pi}{2}\left(\frac{j_d'}{\Omega'} - \frac{j_d}{\Omega}\right)\right], \quad (23)$$

where $\Omega' = \sqrt{j_d'^2 + 4j_x'^2}$.

We now calculate $F_{\min}$ for the controlled π-phase gate. The associated constraint $\phi = \pi/2$ [see Eq. (20)] leads to $n = [2(1 - j_d/\Omega)]^{-1}$. Since n must be an integer, this relation restricts the possible values of δ and Δ_d for fixed values of the charge admixture parameters η_a, η_b and the capacitive coupling strength U_{ab}. For the parameter regime we consider in the present work, we find that n varies more strongly with δ than with Δ_d and set $\Delta_d = 0$ for simplicity in the remainder of the analysis. Choosing $\eta_a = \eta_b \equiv \eta_0 = 0.1$ and $\sigma_s = 2$ μeV,[54] we solve the constraint for the values of δ corresponding to $n = 1, 2, \ldots, 15$ and calculate $F_{\min}$ via numerical integration using Eq. (22). By repeating this calculation for a range of coupling strengths U_{ab}, we obtain the variation of $F_{\min}$ with δ and U_{ab} shown in Fig. 3. We see that $F_{\min}$ increases with increasing coupling strength U_{ab} as expected. For a given value of U_{ab}, $F_{\min}$ also increases as δ increases, i.e., as the energy separation between $|S_{11}, S_{11}\rangle$ and $|S_{02}, S_{02}\rangle$ becomes larger and the contribution of $|S_{02}, S_{02}\rangle$ to the ground state decreases. For $\delta = 41$ μeV (corresponding to $n = 14$) and $U_{ab} = 150$ μeV, $F_{\min} > 0.999$ and the time for the gate $\hat{U}_J$ is $\tau_n = 2\pi n/\Omega \approx 1$ ns.

While we assume ideal echo pulses R_π in the present analysis, switching times for the magnetic gradients used

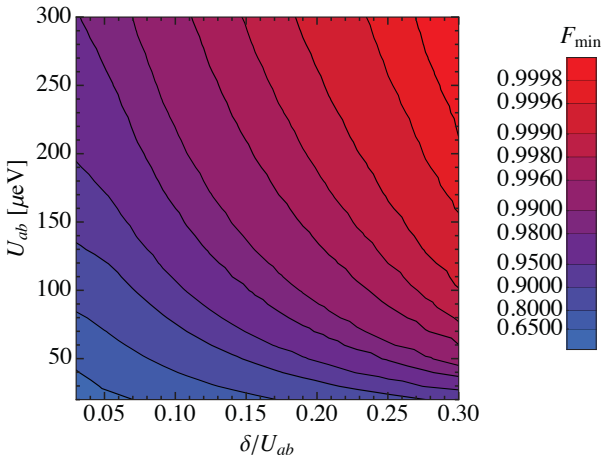

Figure 3. Minimum fidelity $F_{\min}$ [Eq. (22)] of the controlled-phase gate sequence [Eq. (21)] for $\phi = \pi/2$, $\Delta_d = 0$, and $\eta_0 = 0.1$ as a function of the energy difference δ and the capacitive coupling strength U_{ab} [see Fig. 1(b)]. The values of δ in the plot are calculated for each value of U_{ab} by solving the constraint $\phi = \pi/2$ with the chosen parameter values for $n = 1, 2, \ldots, 15$ (see the main text). Note that this implies that the range of δ varies with U_{ab} for fixed η_0. The values of δ are therefore given in units of the value of U_{ab} with which they are associated.

to generate R_π which are longer than the timescale of the qubit dynamics will lead to residual magnetic gradients that remain during the action of the exchange gate $\hat{U}_J$. The residual Zeeman energy $\omega_{Z,\mathrm{res}}$ will modify the Hamiltonian in Eq. (17) and thus lead to errors. Setting $J_a = J_b \equiv J_0$ and assuming $\omega_{Z,\mathrm{res}} \ll J_0$, we can regard the residual magnetic gradient terms as a perturbation to H_J and obtain an upper bound for the allowable residual gradient dB_{res} using the condition $\tau_n \omega_{Z,\mathrm{res}}^2/J_0 \ll 1$. For $\eta_0 = 0.1$, $\delta = 41$ μeV, and $U_{ab} = 150$ μeV, this condition yields $\omega_{Z,\mathrm{res}} \ll 1$ μeV, corresponding to $dB_{\mathrm{res}} \ll 40$ mT for GaAs dots (with $g = -0.44$) and $dB_{\mathrm{res}} \ll 10$ mT for Si dots (with $g = 2$).

V. CHARGE RELAXATION VIA PHONONS

A. Relaxation rate

In addition to charge noise arising from gate voltage fluctuations, charge relaxation due to electron-phonon coupling also affects the coherence of the capacitively coupled double-dot system we consider. Here, we determine the rate Γ of relaxation via phonons that occurs between the eigenstates $|g\rangle$ and $|e\rangle$ of H_{eff} [Eq. (9)], as illustrated in Fig. 2. From Fermi's golden rule, $\Gamma \sim |\langle g| H_{\mathrm{ep}} |e\rangle|^2 \rho(\Omega)$, where H_{ep} is the electron-phonon interaction Hamiltonian and $\rho(\Omega)$ is the phonon density of states at the gap energy Ω. In the following analysis, we consider acoustic phonons in both GaAs and Si quantum dots and calculate Γ for the higher-energy state, assuming $k_B T \lesssim \hbar j_x$. The electron-phonon interaction for GaAs is described by the Hamiltonian[55]

$$H_{\mathrm{GaAs}} = \sum_{\mu,\mathbf{k}} \sqrt{\frac{\hbar}{2\rho_0 V_0 c_\mu k}} \left(k \Xi_l \delta_{\mu,l} - i\beta\right) \times \left(a_{\mu,\mathbf{k}} + a^\dagger_{\mu,-\mathbf{k}}\right) M_k, \tag{24}$$

while the Hamiltonian for Si has the form[56]

$$H_{\mathrm{Si}} = i \sum_{\mu,\mathbf{k}} \sqrt{\frac{\hbar}{2\rho_0 V_0 c_\mu k}} \left(\mathbf{k} \cdot \hat{\boldsymbol{\epsilon}}_{\mu,\mathbf{k}}\, \Xi_d + k_{z'}\, \hat{z}' \cdot \hat{\boldsymbol{\epsilon}}_{\mu,\mathbf{k}}\, \Xi_u\right) \left(a_{\mu,\mathbf{k}} + a^\dagger_{\mu,-\mathbf{k}}\right) M_k. \tag{25}$$

In Eqs. (24) and (25), $a^\dagger_{\mu,\mathbf{k}}$ creates an acoustic phonon with wave vector $\mathbf{k}$, polarization μ [the sum is taken over one longitudinal mode ($\mu = l$) and two transverse modes ($\mu = p$)], phonon speed c_μ, energy $\varepsilon_{\mathrm{ph}} = \hbar c_\mu k$, and unit polarization vector $\hat{\boldsymbol{\epsilon}}_{\mu,\mathbf{k}}$, ρ_0 is the mass density of the material, V_0 is the crystal volume, Ξ_l is the deformation potential and β is the piezoelectric constant for GaAs, Ξ_d (Ξ_u) is the dilation (uniaxial) deformation potential for Si, $\hat{z}'$ denotes the direction of uniaxial strain, and $\delta_{\mu,l}$ is the Kronecker delta function. The different phonon terms appearing in Eqs. (24) and (25) reflect the fact that the crystal structure of GaAs lacks a center of symmetry, whereas unstrained Si has a centrosymmetric crystal structure: while both deformation potential and piezoelectric phonons contribute to the electron-phonon coupling in GaAs, there is no contribution from piezoelectric phonons for Si.[55] Thus, the strength of the electron-phonon coupling and the associated relaxation rate are expected to be much smaller for Si quantum dots.[5]

The factor in H_{GaAs} and H_{Si} encompassing the coupling to electron charge degrees of freedom is $M_k = M_k^{(a)} + M_k^{(b)}$, where

$$M_k^{(\alpha)} \equiv \sum_{i,j=1,2} \sum_\sigma \langle \alpha, i|\, e^{i\mathbf{k}\cdot\mathbf{r}}\, |\alpha, j\rangle\, c^\dagger_{\alpha i\sigma} c_{\alpha j\sigma} \tag{26}$$

and $\mathbf{r}$ is the electron position operator. Note that in our calculation, we take each double dot to be coupled independently to the same phonon bath.[39,43] Thus, we implicitly assume that the phonon mean free path is greater than the size of the system, so that scattering of phonons between interactions with the electron pairs in the two double dots can be neglected. The matrix elements in Eq. (26) depend on the spatial configuration of the four quantum dots and are evaluated using the two-dimensional Gaussian wave functions $\Psi_{\alpha i}(\mathbf{r}) \equiv \langle \mathbf{r}|\alpha, i\rangle = \psi(x - x_{\alpha i})\, \psi(y - y_{\alpha i})$ for $i = 1, 2$ and $\alpha = a, b$, where $\psi(q) = e^{-q^2/4\sigma^2}/\left(2\pi\sigma^2\right)^{1/4}$. Re-expressing $M_k^{(a)}$ and $M_k^{(b)}$ in the basis $\{|S_{11}, S_{11}\rangle, |S_{02}, S_{02}\rangle, |S_{11}, S_{02}\rangle, |S_{02}, S_{11}\rangle\}$ and using the same Schrieffer-Wolff transformation used for H_{hub} in Sec. II to write $\tilde{M}_k = e^{\lambda A} M_k e^{-\lambda A} \approx$

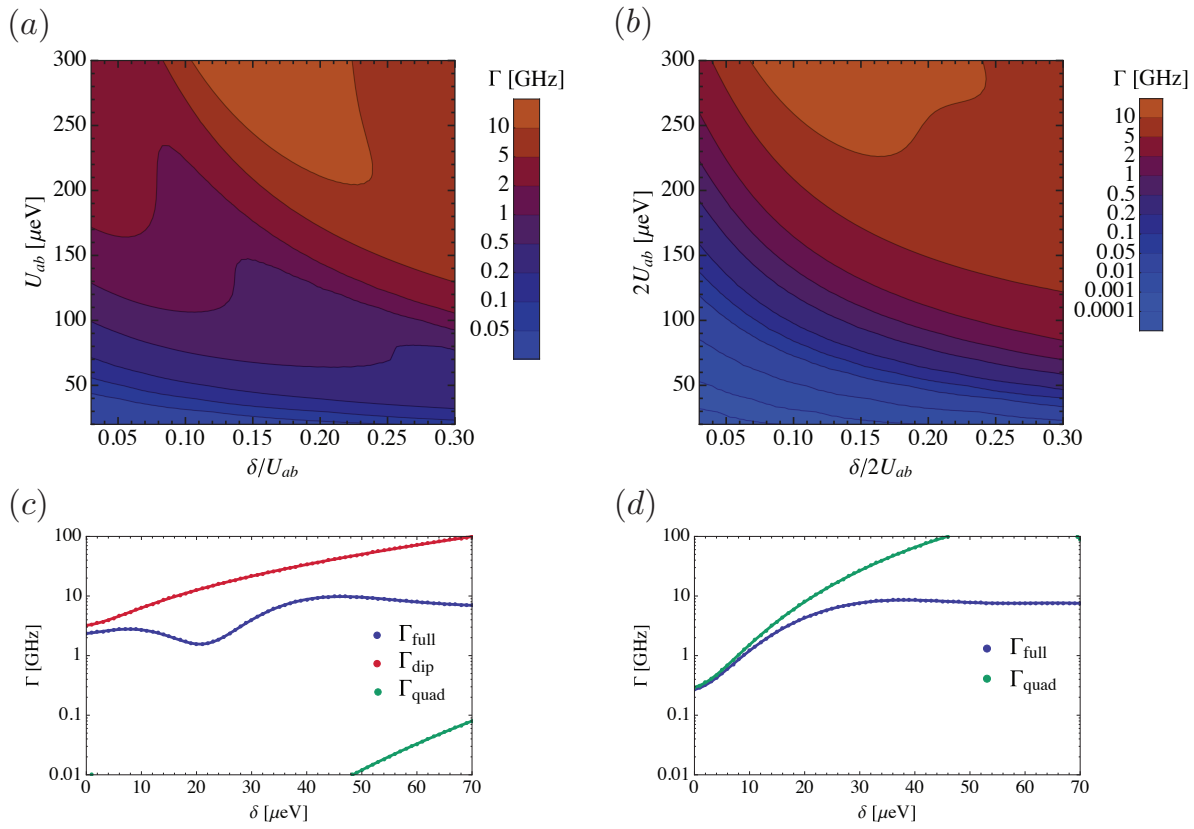

Figure 4. Rate of relaxation via electron-phonon coupling for capacitively coupled GaAs double quantum dots [Eq. (24)]. The rate is calculated as a function of δ and the total interqubit capacitive coupling strength [see Fig. 1(b)], which is equal to U_{ab} for the linear dot geometry (a) and $2U_{ab}$ for the purely quadrupolar dot geometry (b) considered in the present work (see the main text). The parameter values used are $\Delta_d = 0$, $\eta_0 = 0.1$, $d = 140$ nm, $R = 2d$, the GaAs effective mass $m^* = 0.067m_e$ (where m_e is the free-electron mass), dot size $\sigma = 20$ nm, and phonon parameter values $\rho_0 = 5.3 \times 10^3$ kg/m^3, $c_l = 5.3 \times 10^3$ m/s, $c_t = 2.5 \times 10^3$ m/s, $\Xi_l = 7$ eV, and $\beta = 1.4 \times 10^9$ eV/m.[57] (c) Dipolar ($\Gamma_{\rm dip}$) and quadrupolar ($\Gamma_{\rm quad}$) contributions to the full relaxation rate ($\Gamma_{\rm full}$) for the linear geometry of Fig. 1(a) with $U_{ab} = 200$ μeV. (d) Comparison of $\Gamma_{\rm quad}$ and $\Gamma_{\rm full}$ for the purely quadrupolar geometry, corresponding to $\theta = \pi/2$ and $\varphi = 0$ in Fig. 7(a), with $2U_{ab} = 200$ μeV.

$M_k + \lambda\left[A, M_k\right] + \frac{\lambda^2}{2}\left[A,\left[A, M_k\right]\right]$, we determine the transition matrix element

$$\begin{aligned}\langle g|\, M_k\, |e\rangle = \cos\theta \sin\theta \Big(&\langle S_{11}, S_{11}|\, \tilde{M}_k\, |S_{11}, S_{11}\rangle \\ &- \langle S_{02}, S_{02}|\, \tilde{M}_k\, |S_{02}, S_{02}\rangle\Big) \\ &+ \cos^2\theta\, \langle S_{11}, S_{11}|\, \tilde{M}_k\, |S_{02}, S_{02}\rangle \\ &- \sin^2\theta\, \langle S_{02}, S_{02}|\, \tilde{M}_k\, |S_{11}, S_{11}\rangle\,.\end{aligned}$$

The relaxation rates for GaAs and Si are given by $\Gamma_{\rm GaAs} = g_l I\left(\Omega/\hbar c_l\right) + g_p I\left(\Omega/\hbar c_p\right)$ and $\Gamma_{\rm Si} = s_l K_l\left(\Omega/\hbar c_l\right) + s_p K_p\left(\Omega/\hbar c_p\right)$, with the momentum-space angular integrals

$$I(k) \equiv \int |\langle g|\, M_k\, |e\rangle|^2\, d\Omega_{\rm ang}, \tag{27}$$

$$K_l(k) \equiv \int \left(1 + \gamma\cos^2\chi\right)^2 |\langle g|\, M_k\, |e\rangle|^2\, d\Omega_{\rm ang}, \tag{28}$$

$$K_p(k) \equiv \int \gamma^2 \cos^2\chi \sin^2\chi\, |\langle g|\, M_k\, |e\rangle|^2\, d\Omega_{\rm ang} \tag{29}$$

and the factors

$$g_l = \frac{\Omega}{8\pi^2\hbar^2\rho_0 c_l^3}\left(\frac{\Omega^2}{\hbar^2 c_l^2}\Xi_l^2 + \beta^2\right), \tag{30}$$

$$g_p = \frac{2\Omega}{8\pi^2\hbar^2\rho_0 c_p^3}\beta^2, \tag{31}$$

$$s_\mu = \frac{\Omega^3}{8\pi^2\hbar^4\rho_0 c_\mu^5}\Xi_d^2, \quad \mu = l, p. \tag{32}$$

In writing Eqs. (28) and (29), we have chosen one of the two transverse ($\mu = p$) phonon polarization axes to lie orthogonal to $\hat{z}'$ [see Eq. (25)] and defined χ as the angle between $\mathbf{k}$ and $\hat{z}'$. We also define $\gamma \equiv \Xi_u/\Xi_d$, and $\Omega_{\rm ang}$ denotes the momentum-space solid angle.

We calculate the relaxation rates via numerical integration for the linear geometry depicted in Fig. 1(a), which has both dipolar and quadrupolar moments, as well as for a purely quadrupolar geometry, which corresponds to a rectangular arrangement of the dots obtained from the general configuration illustrated in Fig.

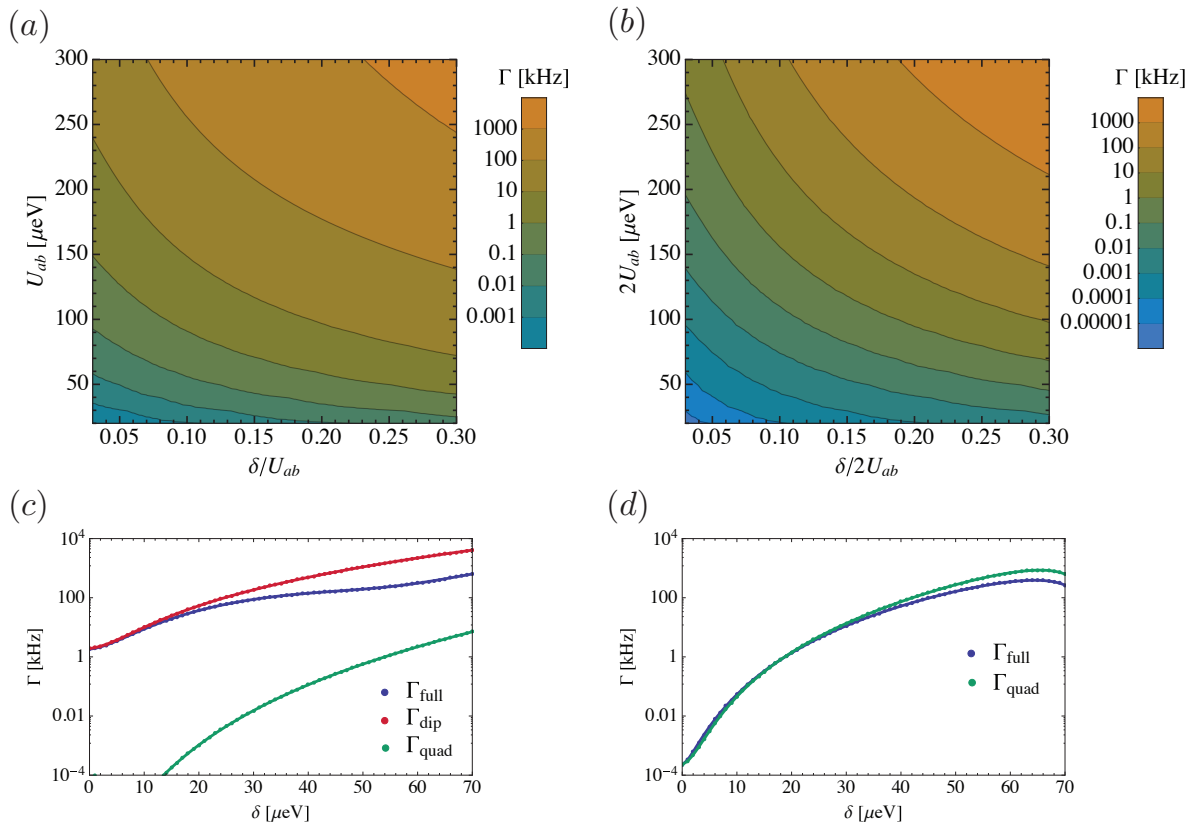

Figure 5. Rate of relaxation via electron-phonon coupling for capacitively coupled Si double quantum dots [Eq. (25)]. The rate is calculated as a function of δ and the total interqubit capacitive coupling strength [see Fig. 1(b)], which is equal to U_{ab} for the linear dot geometry (a) and $2U_{ab}$ for the purely quadrupolar dot geometry (b) considered in the present work (see the main text). The parameter values used are $\Delta_d = 0$, $\eta_0 = 0.1$, $d = 140$ nm, $R = 2d$, the Si effective mass $m^* = 0.19m_e$, dot size $\sigma = 22$ nm, and phonon parameter values $\rho_0 = 2.33 \times 10^3$ kg/m^3, $c_l = 9.33 \times 10^3$ m/s, $c_t = 5.42 \times 10^3$ m/s, $\Xi_d = 5$ eV, and $\Xi_u = 8.77$ eV.[56,58] (c) Dipolar ($\Gamma_{\rm dip}$) and quadrupolar ($\Gamma_{\rm quad}$) contributions to the full relaxation rate ($\Gamma_{\rm full}$) for the linear geometry of Fig. 1(a) with $U_{ab} = 200$ μeV. (d) Comparison of $\Gamma_{\rm quad}$ and $\Gamma_{\rm full}$ for the purely quadrupolar geometry, corresponding to $\theta = \pi/2$ and $\varphi = 0$ in Fig. 7(a), with $2U_{ab} = 200$ μeV.

7(a) by setting $\theta = \pi/2$ and $\varphi = 0$. For the linear case (corresponding to $\theta = 0$, $\varphi = \pi$), we set $x_{a1} = -(R+d)/2$, $x_{a2} = -(R-d)/2$, $x_{b1} = (R-d)/2$, $x_{b2} = (R+d)/2$, and $y_{\alpha i} = 0$ for all α and i. The coordinates of the dot centers for the pure quadrupole are $(x_{a1}, y_{a1}) = (-d/2, R/2)$, $(x_{a2}, y_{a2}) = (d/2, R/2)$, $(x_{b1}, y_{b1}) = (d/2, -R/2)$, $(x_{b2}, y_{b2}) = (-d/2, -R/2)$, and we take as the interqubit Coulomb interaction term for the quadrupolar geometry

$$H_{\rm int} = U_{ab}\left(n_{a2}n_{b1} + n_{a1}n_{b2}\right). \tag{33}$$

Equation (33) leads to $\delta = \Delta_a + \Delta_b - 2U_{ab}$ and corresponding modifications to Eqs. (10)-(13) for the case of the purely quadrupolar system. Note that the total coupling strength between the qubits for the quadrupolar geometry is effectively twice that for the linear geometry. We therefore vary $2U_{ab}$ for the quadrupolar system over the same range of values of U_{ab} considered for the linear configuration, in order to focus on the geometry-dependent variation in the relaxation rate.

The calculated relaxation rates are shown for GaAs in Fig. 4 and for Si in Fig. 5 as a function of δ and the interqubit capacitive coupling strength, where we choose $\Delta_d = 0$, $\eta_0 = 0.1$, $d = 140$ nm, and $R = 2d$. Comparing Figs. 4(a) for the linear geometry and 4(b) for the purely quadrupolar geometry, we see that both relaxation rates increase with increasing U_{ab} but exhibit a nonmonotonic dependence on δ. While the largest rates shown for both geometries are ~ 10 GHz, the rate for the quadrupolar geometry reduces to $\lesssim 100$ kHz for the smallest values of δ and U_{ab} considered. On the other hand, we see from Fig. 4(a) that the rate reduces only to ~ 10 MHz for the linear geometry. Figures 5(a) and 5(b) reveal that the relaxation rates for Si dots are several orders of magnitude smaller than those for GaAs dots, as expected due to the absence of piezoelectric phonons in Si.[5] The rates increase as both U_{ab} and δ are increased, with a maximum rate ~ 1 MHz for the parameter ranges considered. At the smallest values of δ and U_{ab} shown, relaxation for the linear geometry has a rate ~ 1 Hz [Fig. 5(a)], while the rate for the purely quadrupolar geometry [Fig. 5(b)] is two orders of magnitude smaller.

We now consider separately the contributions of the

dipolar and quadrupolar terms in M_k to the total relaxation rates for coupled GaAs and Si double dots in both the linear and the purely quadrupolar geometries. For phonon wavelengths long compared to the size of the quantum dot system, we can write $e^{i\mathbf{k}\cdot\mathbf{r}} \approx 1 + i\mathbf{k}\cdot\mathbf{r} - (\mathbf{k}\cdot\mathbf{r})^2/2$. The dipolar ($\Gamma_{\rm dip}$) and quadrupolar ($\Gamma_{\rm quad}$) contributions to the rate are then obtained by calculating the relaxation rates with the transition matrix elements $\langle g|\, i\mathbf{k}\cdot\mathbf{r}\,|e\rangle$ and $\langle g|\,(\mathbf{k}\cdot\mathbf{r})^2/2\,|e\rangle$, respectively, substituted for the full matrix element $\langle g|\, M_k\,|e\rangle$ in Eqs. (27)-(29). We see in Figs. 4(c) and 5(c) that, for both GaAs and Si, the full relaxation rate $\Gamma_{\rm full}$ for the linear geometry contains a large dipolar contribution and a much smaller quadrupolar contribution. The large dipolar term can be understood from the fact that a net dipole moment exists for the four-electron system in the linear configuration. In contrast, the purely quadrupolar geometry [Figs. 4(d) and 5(d)] lacks a net dipole moment, so that $\Gamma_{\rm dip} = 0$ in this case. While a large discrepancy exists between the quadrupolar contribution $\Gamma_{\rm quad}$ and $\Gamma_{\rm full}$ for GaAs, $\Gamma_{\rm full}$ for Si is well described by the quadrupolar term. This can be understood from the fact that, over the range of δ (and thus Ω) we consider, the ratio of the system size ($\sim R$) to the phonon wavelength is less than 1 for Si. On the other hand, the corresponding ratio for GaAs becomes larger than 1 at sufficiently large values of δ.

B. Modification of controlled-Z gate fidelity

Having calculated the rate of phonon-induced charge relaxation within the two-singlet subspace spanned by $\left\{\left|\widetilde{S_{11}, S_{11}}\right\rangle, \left|\widetilde{S_{02}, S_{02}}\right\rangle\right\}$, we now determine the effect of this decay on the gate fidelity calculated in Sec. IV for the linear quantum dot geometry. In order to incorporate the relaxation into the dynamics, we consider the Lindblad master equation for the density matrix within the two-singlet subspace $\hat{\rho}_s$, which can be written in the form

$$\dot{\hat{\rho}}_s = -i\left[\tilde{H}, \hat{\rho}_s\right] + \Gamma a \hat{\rho}_s a^\dagger \tag{34}$$

with $\hat{a} \equiv \left|\widetilde{S_{11}, S_{11}}\right\rangle\left\langle\widetilde{S_{02}, S_{02}}\right|$ and

$$\tilde{H} \equiv H_{\rm eff} - i\frac{\Gamma}{2}\hat{a}^\dagger\hat{a} = H_{\rm eff} - i\frac{\Gamma}{2}\left|\widetilde{S_{02}, S_{02}}\right\rangle\left\langle\widetilde{S_{02}, S_{02}}\right|. \tag{35}$$

We assume $\Gamma, j_x \ll j_d$ and neglect the final (quantum-jump) term in Eq. (34). Within this approximation, we can regard the dynamics in the two-singlet subspace [Eq. (19)] as being generated by the non-Hermitian "Hamiltonian" in Eq. (35) instead of $H_{\rm eff}$.

We can then estimate the effect of the phonon decay on the dynamics by making the replacements

$$e^{i[(J_a+J_b)\tau_n+\phi]}\left|\widetilde{S_{11}, S_{11}}\right\rangle\left\langle\widetilde{S_{11}, S_{11}}\right| \rightarrow e^{-\Gamma_{\rm eff}\tau_n}e^{i[(J_a+J_b)\tau_n+\phi]}\left|\widetilde{S_{11}, S_{11}}\right\rangle\left\langle\widetilde{S_{11}, S_{11}}\right|,$$
$$e^{i[(J_a+J_b)\tau_n+\phi]}\left|\widetilde{S_{02}, S_{02}}\right\rangle\left\langle\widetilde{S_{02}, S_{02}}\right| \rightarrow e^{-\Gamma_2\tau_n}e^{i[(J_a+J_b)\tau_n+\phi]}\left|\widetilde{S_{02}, S_{02}}\right\rangle\left\langle\widetilde{S_{02}, S_{02}}\right|$$

in $\hat{U}_J(\tau_n)$ [see Eq. (18)]. Here, $\Gamma_{\rm eff} \equiv \Gamma j_x^2/2j_d^2$ and the explicit form of Γ_2 does not enter into the calculation for our choice of initial state $|\psi_{\rm in}\rangle$, which is defined entirely within the effective $|1111\rangle$ subspace. Incorporating these modifications into the gate sequence in Eq. (21), we determine the resulting modified minimum gate fidelity $F'_{\rm min}$ using Eq. (22).

The results are shown in Fig. 6(a) for GaAs dots and in Fig. 6(b) for Si dots. Comparing these plots with Fig. 3, we see that the phonon-induced decay results in a large reduction of the gate fidelity for GaAs, as expected from the fact that $\Gamma_{\rm GaAs} \sim 100$ MHz $-$ 10 GHz is comparable to $1/\tau_n$. In contrast, essentially no modification to the fidelity occurs for the case of Si, since $\Gamma_{\rm Si} \lesssim 1$ MHz $\ll 1/\tau_n$. Thus, we find that an implementation of the controlled-Z gate based on Si quantum dots provides robustness to phonon-induced decay.

While the analysis so far has assumed quasistatic charge noise, fast charge noise also affects the coherence of singlet-triplet spin qubits in practice.[42] Accordingly, we also calculate the modified minimum fidelity $F''_{\rm min}$ of the controlled-phase gate in the presence of decay with an effective rate $\Gamma'_{\rm eff} \equiv \Gamma_{\rm eff} + \Gamma_{\rm chg}$, where $\Gamma_{\rm chg}$ is the fast charge noise frequency. Note that, for realistic devices, $\Gamma_{\rm chg}$ may vary with the particular operating point via the dependence of the detuning noise spectral density on this point.[42] Here, we assume that $\Gamma_{\rm chg}$ is independent of the operating point for simplicity. The results for GaAs (Si) dots are shown for $\Gamma_{\rm chg} = 1$ MHz (representing the high-frequency limit of the noise spectra analyzed in Ref. 42) in Fig. 6(c) [Fig. 6(d)] and for $\Gamma_{\rm chg} = 1$ GHz in Fig. 6(e) [Fig. 6(f)]. We find that, while the gate fidelity for GaAs dots is further degraded in the presence of fast charge noise, fidelities of up to $F''_{\rm min} \sim 0.999$ are in principle possible for Si dots even in the presence of 1 MHz charge noise. Charge noise of frequency $\Gamma_{\rm chg} = 1$ GHz results in a significant reduction of the gate fidelity for Si dots, which becomes similar to that for GaAs dots with $\Gamma_{\rm chg} = 1$ GHz [Fig. 6(e)] as expected from the fact that $\Gamma_{\rm Si} \ll 1$ GHz [see Fig. 5(a)].

VI. DEPENDENCE OF CAPACITIVE COUPLING ON DOT GEOMETRY

Finally, we consider how the capacitive coupling strength varies with the relative orientation of the double dots.[53] Specifically, we consider the geometry shown in

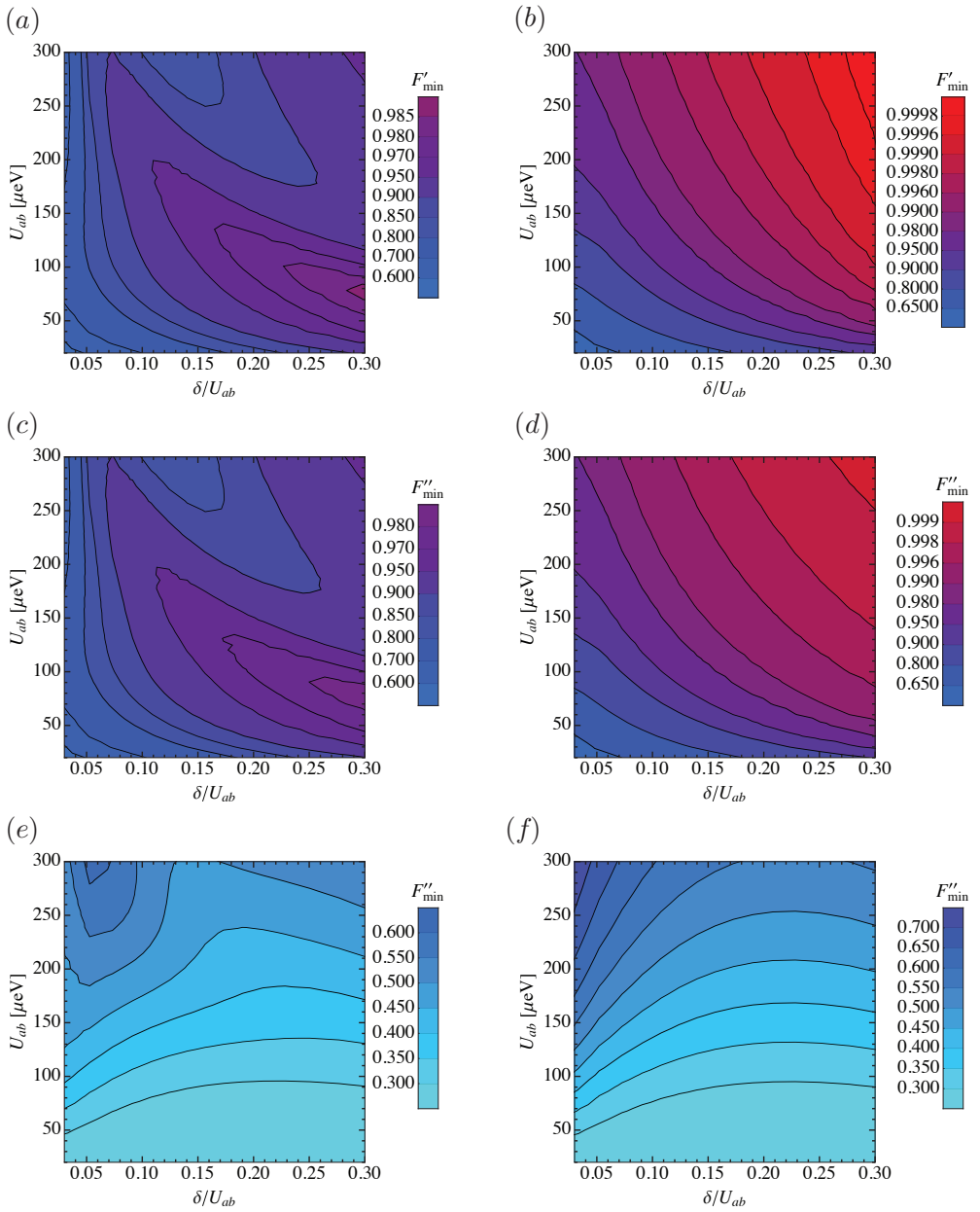

Figure 6. (a),(b) Modified minimum fidelity $F'_{\min}$ of the controlled-phase gate sequence [Eq. (21)] for $\phi = \pi/2$, in the presence of decay due to electron-phonon coupling in (a) GaAs and (b) Si quantum dots arranged in the linear geometry of Fig. 1(a). The parameters used in the calculation are identical to those given in the captions of Figs. 3,4, and 5. (c)-(f) Modified minimum fidelity $F''_{\min}$ in the presence of both phonon-induced decay and charge noise of frequency $\Gamma_{\rm chg}$, calculated for (c) GaAs dots with $\Gamma_{\rm chg} = 1$ MHz, (d) Si dots with $\Gamma_{\rm chg} = 1$ MHz, (e) GaAs dots with $\Gamma_{\rm chg} = 1$ GHz, and (f) Si dots with $\Gamma_{\rm chg} = 1$ GHz.

Fig. 7(a) and the general form of the capacitive interaction term in the Hamiltonian, given by

$$H_C = \frac{1}{2}\sum_{i\neq j} U_{ij} n_i n_j. \tag{36}$$

In Eq. (36), we have for notational convenience redefined the dot indices $a1, a2, b1$, and $b2$ as $1, 2, 3$, and 4, respectively. The matrix element of the Coulomb interaction between the electrons in dot i and dot j with center positions $\mathbf{R}_i = (x_i, y_i)$ and $\mathbf{R}_j = (x_j, y_j)$, respectively, is[55]

$$\begin{aligned} U_{ij} &\equiv \langle ij| \frac{1}{r} |ij\rangle \\ &\equiv \int \frac{|\Psi_i(\mathbf{r})|^2 |\Psi_j(\mathbf{r}')|^2}{|\mathbf{r}-\mathbf{r}'|} d\mathbf{r} d\mathbf{r}', \end{aligned} \tag{37}$$

where $\Psi_i(\mathbf{r}) \equiv \langle \mathbf{r}|i\rangle = \psi(x - x_i)\,\psi(y - y_i)$ and ψ is the one-dimensional Gaussian function defined in Sec. V. We assume $R \gg d$ [see Fig. 7(a)] and estimate U_{ij} by

the leading order term in the multipole expansion of the Coulomb interaction as

$$U_{ij} \sim \frac{1}{|\mathbf{R}_i - \mathbf{R}_j|}. \tag{38}$$

Defining $E(n_1\ n_2\ n_3\ n_4)$ as the energy of the charge state $|n_1\ n_2\ n_3\ n_4\rangle$, the Coulomb energy that sets the speed of the controlled-Z gate in the double charge resonant regime is given by

$$\begin{aligned} U_{0202} &\equiv E(0202) - E(1111) - [E(0211) - E(1111)] \\ &\quad - [E(1102) - E(1111)] \\ &= E(0202) + E(1111) - E(0211) - E(1102) \\ &= U_{13} + U_{24} - U_{14} - U_{23}. \end{aligned} \tag{39}$$

We note that Eq. (39) includes the term $U_{23} = U_{ab}$, which is the dominant term in U_{0202} for the parameter regime we consider in the present work. U_{0202} depends on the parameters R, d, θ, and φ through Eq. (38).

The dependence of U_{0202} on the relative orientation of the two double dots, determined by θ and φ [see Fig. 7(a)], is shown in Fig. 7(b) for fixed R/d. From this dependence, we see that the linear geometry ($\theta = 0$, $\varphi = \pi$) is associated with a minimum energy, corresponding to an attractive dipole-dipole interaction of maximum strength, and therefore provides the fastest gate. On the other hand, the case $\theta = 0$, $\varphi = 0$ corresponds to a maximum repulsive interaction strength.

Note that Eq. 38 is approximately independent of the dot size σ. Thus, to leading order, the interqubit capacitive coupling strength for $R \gg d$ is largely insensitive to variations in the sizes of the dots and depends primarily on the dot center positions. While the sensitivity of the intraqubit tunneling amplitudes to dot size differences may modify the charge admixture η_α and thus lead to changes in the gate speed, this sensitivity will not qualitatively affect the approach discussed in the present work. In addition, knowledge of the dot size variation should in principle enable tuning of the gate voltages controlling the double dot potentials in order to compensate for changes in the intraqubit charge admixture and thereby optimize the fidelity.

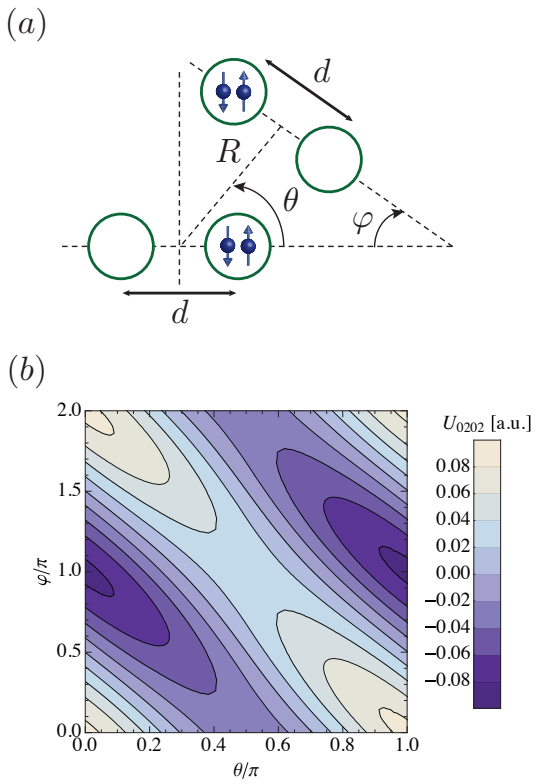

Figure 7. (a) Illustration of a pair of double dots having interdot distance d, separated by distance R, and with relative in-plane orientation determined by the angles θ and φ. (b) Variation of the capacitive coupling U_{0202} [Eq. (39)] with θ and φ for $R/d = 3$.

VII. CONCLUSIONS

In the present work, we have investigated capacitively coupled singlet-triplet qubits in a pair of adjacent double quantum dots in the double charge resonant regime, where the interqubit Coulomb interaction leads to near-degeneracy between the $|1111\rangle$ and $|0202\rangle$ charge states. This regime is different from that considered in Ref. 2 and subsequent work, where the two-qubit coupling relies on a repulsive dipole-dipole interaction. Using the dynamics generated within the two-singlet subspace by the capacitive coupling, we derived a sequence for a controlled-phase gate that includes spin echo pulses to correct for single-qubit dephasing. For this gate sequence, we showed that rapid gates with fidelities greater than 0.9998 in the presence of classical, static charge noise are in principle achievable by adjusting the individual qubit detunings to appropriate values. We also studied the relaxation of coupled singlet-triplet qubits via electron-phonon interaction for quantum dots in both GaAs and Si. The full relaxation rates, as well as their dipolar and quadrupolar contributions, were calculated for both linear and purely quadrupolar dot geometries. For the linear dot geometry, we showed that the presence of phonon-induced decay results in a large decrease in the gate fidelity for GaAs dots but does not significantly affect the fidelity in the case of Si dots due to much slower charge relaxation. In addition, we found that fidelities greater than 0.999 are in principle possible for Si dots even in the presence of 1 MHz charge noise. Finally, we showed that the linear geometry gives rise to the fastest two-qubit gate.

These results demonstrate that the intraqubit detunings, interqubit interaction strengths, and geometry of a capacitively coupled pair of double dots can be chosen in order to optimize the controlled-Z gate fidelity. Implementations of this gate in the double charge resonant

regime using Si dots arranged in a linear geometry should lead to high fidelities in the presence of both quasistatic and fast charge noise as well as relaxation via phonons. Improvements to the results of the present work might be found by considering the double charge resonant regime for, e.g., multi-electron singlet-triplet qubits,[59–62] which are expected to have enhanced robustness to charge noise due to screening of the Coulomb interaction by the additional electrons in the dots. Finally, we note that measured relations for the exchange coupling as a function of detuning in double dots[20,42] deviate from the detuning dependence in Eqs. (10) and (11) derived from the Hubbard model and thus may lead to different optimal operating points for the controlled-phase gate. Potential future directions therefore also include exploring extensions to the Hubbard model as well as more sophisticated charge noise models[34,36] in order to obtain a more accurate description of capacitively coupled double dots in the double charge resonant regime.

ACKNOWLEDGMENTS

We acknowledge useful discussions with A. Yacoby, S. Das Sarma, B. Halperin, A. Pal, and S. Yang. We also thank M. Maghrebi and G. Solomon for helpful comments. This work was supported by DARPA MTO and the NSF-funded Physics Frontier Center at the JQI.

Appendix A: Basis states obtained via Schrieffer-Wolff transformation

Here, we give expressions for the corrected states resulting from the Schrieffer-Wolff transformation used to obtain the effective Hamiltonian $H_{\rm eff}$ [Eq. (9)]. Up to second order in the charge admixture parameters η_a and η_b defined in Sec. II, we find

$$\begin{aligned}\left|\widetilde{S_{11},S_{11}}\right\rangle \approx{}& \left(1-\eta_a^2-\eta_b^2\right)|S_{11},S_{11}\rangle \\ &-2\eta_a\eta_b\frac{\left(U_{ab}^2-\delta^2+\Delta_d^2\right)}{\left(U_{ab}-\delta\right)^2-\Delta_d^2}|S_{02},S_{02}\rangle \\ &+\sqrt{2}\eta_b|S_{11},S_{02}\rangle+\sqrt{2}\eta_a|S_{02},S_{11}\rangle\,, \end{aligned} \tag{A1}$$

$$\begin{aligned}\left|\widetilde{S_{02},S_{02}}\right\rangle \approx{}& \left[1-\eta_a^2\frac{\left(U_{ab}+\delta+\Delta_d\right)^2}{\left(U_{ab}-\delta-\Delta_d\right)^2}\right. \\ &\left.-\eta_b^2\frac{\left(U_{ab}+\delta-\Delta_d\right)^2}{\left(U_{ab}-\delta+\Delta_d\right)^2}\right]|S_{02},S_{02}\rangle \\ &-2\eta_a\eta_b\frac{\left(U_{ab}^2-\delta^2+\Delta_d^2\right)}{\left(U_{ab}-\delta\right)^2-\Delta_d^2}|S_{11},S_{11}\rangle \\ &+\sqrt{2}\eta_a\frac{\left(U_{ab}+\delta+\Delta_d\right)}{\left(U_{ab}-\delta-\Delta_d\right)}|S_{11},S_{02}\rangle \\ &+\sqrt{2}\eta_b\frac{\left(U_{ab}+\delta-\Delta_d\right)}{\left(U_{ab}-\delta+\Delta_d\right)}|S_{02},S_{11}\rangle\,, \end{aligned} \tag{A2}$$

$$\begin{aligned}\left|\widetilde{S_{11},S_{02}}\right\rangle \approx{}& \left[1-\eta_a^2\frac{\left(U_{ab}+\delta+\Delta_d\right)^2}{\left(U_{ab}-\delta-\Delta_d\right)^2}-\eta_b^2\right]|S_{11},S_{02}\rangle \\ &-2\eta_a\eta_b\frac{\left(U_{ab}^2+\delta^2-\Delta_d^2\right)}{\left(U_{ab}-\delta\right)^2-\Delta_d^2}|S_{02},S_{11}\rangle \\ &-\sqrt{2}\eta_b|S_{11},S_{11}\rangle \\ &-\sqrt{2}\eta_a\frac{\left(U_{ab}+\delta+\Delta_d\right)}{\left(U_{ab}-\delta-\Delta_d\right)}|S_{02},S_{02}\rangle\,, \end{aligned} \tag{A3}$$

$$\begin{aligned}\left|\widetilde{S_{02},S_{11}}\right\rangle \approx{}& \left[1-\eta_a^2-\eta_b^2\frac{\left(U_{ab}+\delta-\Delta_d\right)^2}{\left(U_{ab}-\delta+\Delta_d\right)^2}\right]|S_{02},S_{11}\rangle \\ &-2\eta_a\eta_b\frac{\left(U_{ab}^2+\delta^2-\Delta_d^2\right)}{\left(U_{ab}-\delta\right)^2-\Delta_d^2}|S_{11},S_{02}\rangle \\ &-\sqrt{2}\eta_a|S_{11},S_{11}\rangle \\ &-\sqrt{2}\eta_b\frac{\left(U_{ab}+\delta-\Delta_d\right)}{\left(U_{ab}-\delta+\Delta_d\right)}|S_{02},S_{02}\rangle\,. \end{aligned} \tag{A4}$$

Appendix B: Minimum fidelity

The expression in Eq. (23) for the minimum fidelity of the controlled π-phase (or controlled-Z) gate is obtained using the particular state $|\psi_{\rm in}\rangle$ chosen for the analysis in the present work. Here, we show that this initial state represents only one possible element of a more general class of states that minimize the gate fidelity (and thus maximize the error) for a given charge noise distribution. We write $\hat{\rho}_{\rm out}^{(0)}\equiv U_\phi|\psi\rangle\langle\psi|U_\phi^\dagger$ and $\hat{\rho}_{\rm out}\equiv U'_\phi|\psi\rangle\langle\psi|U_\phi'^\dagger$ for an arbitrary initial state $|\psi\rangle\equiv c_{TT}|T_{11},T_{11}\rangle+c_{ST}\left|\tilde{S}_{11},T_{11}\right\rangle+c_{TS}\left|T_{11},\tilde{S}_{11}\right\rangle+c_{SS}\left|\widetilde{S_{11},S_{11}}\right\rangle$, where c_{TT}, c_{ST}, c_{TS}, and c_{SS} are complex coefficients. The gate fidelity then becomes [see Eq. (22)]

$$\begin{aligned} f &\equiv {\rm Tr}\left[\hat{\rho}_{\rm out}^{(0)}\hat{\rho}_{\rm out}\right] \\ &= \left|\langle\psi|U_\phi^\dagger U'_\phi|\psi\rangle\right|^2 \\ &= A^2+B^2+2AB\cos\left[n\pi\left(\frac{j'_d}{\Omega'}-\frac{j_d}{\Omega}\right)\right], \end{aligned} \tag{B1}$$

with $A\equiv|c_{TT}|^2+|c_{SS}|^2$ and $B\equiv|c_{TS}|^2+|c_{ST}|^2$. Noting that the minimum value of the cosine function is -1, we then find $f_{\rm min}=A^2+B^2-2AB=(A-B)^2$. This has a minimum value of zero for $A=B$. Together with the normalization condition $A+B=1$ for $|\psi\rangle$, this yields $A=B=1/2$, so that

$$\begin{aligned} f_{\rm min} &= \frac{1}{2}+\frac{1}{2}\cos\left[n\pi\left(\frac{j'_d}{\Omega'}-\frac{j_d}{\Omega}\right)\right] \\ &= \cos^2\left[\frac{n\pi}{2}\left(\frac{j'_d}{\Omega'}-\frac{j_d}{\Omega}\right)\right], \end{aligned} \tag{B2}$$

which agrees with the expression for the minimum fidelity in Eq. (23) determined

using the specific input state $|\psi_{\rm in}\rangle = \frac{1}{2}\left(|T_{11},T_{11}\rangle + \left|\tilde{S}_{11},T_{11}\right\rangle + \left|T_{11},\tilde{S}_{11}\right\rangle + \left|\widetilde{S_{11},S_{11}}\right\rangle\right)$. Note that for this state, $c_{TT} = c_{SS} = c_{TS} = c_{ST} = 1/2$, which satisfies $A = B = 1/2$. Thus, $|\psi_{\rm in}\rangle$ represents a particular initial state that minimizes the gate fidelity. All such states lead to the same expression for $f_{\rm min}$ [Eq. (B2)].

* vsriniv@umd.edu

[1] D. Loss and D. P. DiVincenzo, Phys. Rev. A **57**, 120 (1998).
[2] J. M. Taylor, H. A. Engel, W. Dur, A. Yacoby, C. M. Marcus, P. Zoller, and M. D. Lukin, Nature Phys. **1**, 177 (2005).
[3] R. Hanson, L. P. Kouwenhoven, J. R. Petta, S. Tarucha, and L. M. K. Vandersypen, Rev. Mod. Phys. **79**, 1217 (2007).
[4] C. Kloeffel and D. Loss, Annual Review of Condensed Matter Physics **4**, 51 (2013).
[5] F. A. Zwanenburg, A. S. Dzurak, A. Morello, M. Y. Simmons, L. C. L. Hollenberg, G. Klimeck, S. Rogge, S. N. Coppersmith, and M. A. Eriksson, Rev. Mod. Phys. **85**, 961 (2013).
[6] G. Burkard, D. Loss, and D. P. DiVincenzo, Phys. Rev. B **59**, 2070 (1999).
[7] J. Levy, Phys. Rev. Lett. **89**, 147902 (2002).
[8] J. M. Taylor, J. R. Petta, A. C. Johnson, A. Yacoby, C. M. Marcus, and M. D. Lukin, Phys. Rev. B **76**, 035315 (2007).
[9] J. R. Petta, A. C. Johnson, J. M. Taylor, E. A. Laird, A. Yacoby, M. D. Lukin, C. M. Marcus, M. P. Hanson, and A. C. Gossard, Science **309**, 2180 (2005).
[10] M. Pioro-Ladriere, T. Obata, Y. Tokura, Y. S. Shin, T. Kubo, K. Yoshida, T. Taniyama, and S. Tarucha, Nature Phys. **4**, 776 (2008).
[11] S. Foletti, H. Bluhm, D. Mahalu, V. Umansky, and A. Yacoby, Nature Phys. **5**, 903 (2009).
[12] A. C. Johnson, J. R. Petta, J. M. Taylor, A. Yacoby, M. D. Lukin, C. M. Marcus, M. P. Hanson, and A. C. Gossard, Nature **435**, 925 (2005).
[13] J. M. Taylor, W. Dür, P. Zoller, A. Yacoby, C. M. Marcus, and M. D. Lukin, Phys. Rev. Lett. **94**, 236803 (2005).
[14] F. H. L. Koppens, J. A. Folk, J. M. Elzerman, R. Hanson, L. H. W. van Beveren, I. T. Vink, H. P. Tranitz, W. Wegscheider, L. P. Kouwenhoven, and L. M. K. Vandersypen, Science **309**, 1346 (2005).
[15] W. A. Coish and D. Loss, Phys. Rev. B **72**, 125337 (2005).
[16] E. A. Laird, J. R. Petta, A. C. Johnson, C. M. Marcus, A. Yacoby, M. P. Hanson, and A. C. Gossard, Phys. Rev. Lett. **97**, 056801 (2006).
[17] H. Bluhm, S. Foletti, I. Neder, M. Rudner, D. Mahalu, V. Umansky, and A. Yacoby, Nature Phys. **7**, 109 (2011).
[18] X. Wang, L. S. Bishop, J. P. Kestner, E. Barnes, K. Sun, and S. Das Sarma, Nat. Commun. **3**, 997 (2012).
[19] C. Barthel, J. Medford, C. M. Marcus, M. P. Hanson, and A. C. Gossard, Phys. Rev. Lett. **105**, 266808 (2010).
[20] B. M. Maune, M. G. Borselli, B. Huang, T. D. Ladd, P. W. Deelman, K. S. Holabird, A. A. Kiselev, I. Alvarado-Rodriguez, R. S. Ross, A. E. Schmitz, M. Sokolich, C. A. Watson, M. F. Gyure, and A. T. Hunter, Nature **481**, 344 (2012).
[21] X. Wu, D. R. Ward, J. R. Prance, D. Kim, J. K. Gamble, R. T. Mohr, Z. Shi, D. E. Savage, M. G. Lagally, M. Friesen, S. N. Coppersmith, and M. A. Eriksson, Proc. Nat. Acad. Sci. USA **111**, 11938 (2014).
[22] I. van Weperen, B. D. Armstrong, E. A. Laird, J. Medford, C. M. Marcus, M. P. Hanson, and A. C. Gossard, Phys. Rev. Lett. **107**, 030506 (2011).
[23] M. D. Shulman, O. E. Dial, S. P. Harvey, H. Bluhm, V. Umansky, and A. Yacoby, Science **336**, 202 (2012).
[24] J. Klinovaja, D. Stepanenko, B. I. Halperin, and D. Loss, Phys. Rev. B **86**, 085423 (2012).
[25] R. Li, X. Hu, and J. Q. You, Phys. Rev. B **86**, 205306 (2012).
[26] J. P. Kestner, X. Wang, L. S. Bishop, E. Barnes, and S. Das Sarma, Phys. Rev. Lett. **110**, 140502 (2013).
[27] M. P. Wardrop and A. C. Doherty, Phys. Rev. B **90**, 045418 (2014).
[28] S. Mehl, H. Bluhm, and D. P. DiVincenzo, Phys. Rev. B **90**, 045404 (2014).
[29] W. G. van der Wiel, S. De Franceschi, J. M. Elzerman, T. Fujisawa, S. Tarucha, and L. P. Kouwenhoven, Rev. Mod. Phys. **75**, 1 (2002).
[30] R. Hanson and G. Burkard, Phys. Rev. Lett. **98**, 050502 (2007).
[31] D. Stepanenko and G. Burkard, Phys. Rev. B **75**, 085324 (2007).
[32] G. Ramon, Phys. Rev. B **84**, 155329 (2011).
[33] L. Trifunovic, O. Dial, M. Trif, J. R. Wootton, R. Abebe, A. Yacoby, and D. Loss, Phys. Rev. X **2**, 011006 (2012).
[34] E. Nielsen, R. P. Muller, and M. S. Carroll, Phys. Rev. B **85**, 035319 (2012).
[35] X. Wang, E. Barnes, and S. Das Sarma, arXiv:1412.7756v2 (2014).
[36] F. A. Calderon-Vargas and J. P. Kestner, Phys. Rev. B **91**, 035301 (2015).
[37] G. Burkard and A. Imamoglu, Phys. Rev. B **74**, 041307 (2006).
[38] J. M. Taylor and M. D. Lukin, arXiv:cond-mat/0605144 (2006).
[39] S. D. Barrett and C. H. W. Barnes, Phys. Rev. B **66**, 125318 (2002).
[40] X. Hu and S. Das Sarma, Phys. Rev. Lett. **96**, 100501 (2006).
[41] D. Culcer, X. Hu, and S. Das Sarma, Applied Physics Letters **95**, 073102 (2009).
[42] O. E. Dial, M. D. Shulman, S. P. Harvey, H. Bluhm, V. Umansky, and A. Yacoby, Phys. Rev. Lett. **110**, 146804 (2013).
[43] T. Brandes and T. Vorrath, Phys. Rev. B **66**, 075341 (2002).
[44] T. Meunier, I. T. Vink, L. H. Willems van Beveren, K.-J. Tielrooij, R. Hanson, F. H. L. Koppens, H. P. Tranitz, W. Wegscheider, L. P. Kouwenhoven, and L. M. K. Vandersypen, Phys. Rev. Lett. **98**, 126601 (2007).
[45] C. Barthel, J. Medford, H. Bluhm, A. Yacoby, C. M. Marcus, M. P. Hanson, and A. C. Gossard, Phys. Rev. B **85**, 035306 (2012).

[46] M. Raith, P. Stano, and J. Fabian, Phys. Rev. B **86**, 205321 (2012).
[47] J. Danon, Phys. Rev. B **88**, 075306 (2013).
[48] F. R. Braakman, J. Danon, L. R. Schreiber, W. Wegscheider, and L. M. K. Vandersypen, Phys. Rev. B **89**, 075417 (2014).
[49] S. Yang, X. Wang, and S. Das Sarma, Phys. Rev. B **83**, 161301 (2011).
[50] L. M. K. Vandersypen and I. L. Chuang, Rev. Mod. Phys. **76**, 1037 (2005).
[51] L.-A. Wu and D. A. Lidar, Phys. Rev. Lett. **88**, 207902 (2002).
[52] T. Meunier, V. E. Calado, and L. M. K. Vandersypen, Phys. Rev. B **83**, 121403 (2011).
[53] S. Yang and S. Das Sarma, Phys. Rev. B **84**, 121306 (2011).
[54] K. D. Petersson, J. R. Petta, H. Lu, and A. C. Gossard, Phys. Rev. Lett. **105**, 246804 (2010).
[55] G. Mahan, *Many-Particle Physics* (Plenum, 1990).
[56] P. Yu and M. Cardona, *Fundamentals of Semiconductors: Physics and Materials Properties*, Graduate Texts in Physics (Springer, 2010).
[57] P. Stano and J. Fabian, Phys. Rev. Lett. **96**, 186602 (2006).
[58] C. Tahan and R. Joynt, Phys. Rev. B **89**, 075302 (2014).
[59] S. Vorojtsov, E. R. Mucciolo, and H. U. Baranger, Phys. Rev. B **69**, 115329 (2004).
[60] E. Barnes, J. P. Kestner, N. T. T. Nguyen, and S. Das Sarma, Phys. Rev. B **84**, 235309 (2011).
[61] A. P. Higginbotham, F. Kuemmeth, M. P. Hanson, A. C. Gossard, and C. M. Marcus, Phys. Rev. Lett. **112**, 026801 (2014).
[62] S. Mehl and D. P. DiVincenzo, Phys. Rev. B **88**, 161408 (2013).